JOURNAL OF MATERIALS SCIENCE 13 (1978) 2650–2658

The mechanical behaviour of porous austenitic stainless steel fibre structures

PAUL DUCHEYNE*, ETIENNE AERNOUDT, PAUL DE MEESTER
Katholieke Universiteit Leuven, Department of Metallurgy, de Croylaan 2, B-3030 Heverlee, Belgium

The mechanical properties of metal fibre porous structures were studied in the light of their potential application as surface coatings of implants. Stainless steel AISI 316 L fibres with diameters of 50 and 100 μm were compacted and sintered. The variation of the modulus of elasticity with density, as obtained in tension, corresponds closely with theoretical models. The ultimate failure of the tensile specimens proceeds through the fibres, and not through the sinter bonds, except at lower densities. Differences in yield strength between 50 and 100 μm fibre tensile specimens are explained on the basis of the onset of plastic deformation of the individual fibres. Upon compression the modulus of elasticity is nearly 10 times smaller than in tension. This result is due to the different deformation patterns of the fibres in compression and tension.

1. Introduction

An area of powder metallurgy which has gained increasing interest is the development of porous metal products [1]. Contrary to the objective of most powder metallurgical work, where the obtention of a structure as dense as possible is paramount, the development of porous products has focused on the production of a material with controlled pore size and porosity. Properties that have been studied depend upon the application of the porous material and include for instance a suitable permeability for filters [1], a high porosity for batteries and a high wear resistance for bearings [2].

A potential application for porous materials is the use as surgical implants. Permanent orthopaedic implants are now stabilized with regard to the skeleton by techniques which are not completely satisfactory [3, 4]. A new fixation method is based on the principle of mechanical interlocking of bone and implant by osseous ingrowth into surface pores of the implant [5].

Several materials and techniques were considered in order to obtain porous structures with suitable properties. Titanium substrates were coated by plasma-spraying of titanium hydride powders [6]; atomized spherical cast cobalt–chromium alloy powders were applied to a metal substrate by aqueous slurry coating and subsequent sintering [7]; stainless steel AISI 316 L powders were isostatically compacted [8]; "void metal composites" were developed by mixing titanium powder with a metal powder with a low melting point, which vaporized upon sintering [9]; fine titanium wires [10] and stainless steel AISI 316 L [11] were compacted either uniaxially or isostatically. Much attention was paid to producing a sufficiently large pore size, since it had been shown that viable bone ingrowth only occurred when the mean pore size was at least 50 μm [12, 13].

The assessment of some mechanical and especially the elastic properties of the porous structures for bone ingrowth is, however, as important from several points of view. Firstly, the orthopaedic prostheses for which the fixation by bone ingrowth is being studied are load bearing prostheses. Peak loads up to 11 or 7 times body weight can occur in the human hip or knee joint respectively [14]. These joints are the more im-

* "Aangesteld navorser NFWO" (Affiliated with the Belgium Foundation for Scientific Research).

portant candidates for replacements by prostheses attached to the remaining bone by osseus infiltration.

Eventually, the repetitve application of high loads in the hip joint can lead to a metal fatigue failure of the implanted protheses [15, 16]. Candidate protheses have been composed of a dense metal substrate coated by a porous layer, allowing bone ingrowth. The characterization of the mechanical properties of the porous structures is necessary to determine the maximum allowable stresses in the coating. Secondly, upon firm fixation stresses are transferred from the prosthesis to the surrounding bone. The compliance of the dense metal core, the porous coating and the surrounding bone varies over two orders of magnitude: the modulus of elasticity of a 100% dense stainless steel AISI 316 L prosthetic substrate is $200\,GN\,m^{-2}$ and the modulus of the trabecular bone which surrounds the prosthesis has a mean value of 0.50 to $1.50\,GN\,m^{-2}$ depending upon the density and the structure [17, 18]. The knowledge of the modulus of elasticity of the porous structure is essential to assess the shear stress at the elastically discontinuous interfaces [19].

The present paper deals with the determination of some mechanical properties of the porous metal fibre structures developed by the present authors [11]. Tension tests perpendicular to and compression tests parallel with the direction of compaction were performed, yielding results for the modulus of elasticity, the yield stress, the ultimate tensile strength and the failure mode as a function of the porosity.

2. Materials and methods

Flat tensile specimens were compacted uniaxially, perpendicular to their longitudinal axis. Stainless steel fibres type AISI 316 L with a length of 4 mm and a diameter of 50 to 100 μm were used. A large variation in density was obtained. The compaction pressure as a function of the density after sintering is shown in Table I.

The thickness of the specimens varied with the density. The width and the length of the specimens is shown in Fig. 1. After compaction the 50 μm fibre specimens were sintered in a high purity hydrogen atmosphere for 2 h, and 100 μm fibre specimens for 4 h at 1250° C. The density of each specimen was determined geometrically. Tensile testing was carried out on an Instron TT-DM-L machine. An extensometer with a span of 25 mm and a range of 10% was used. This means that at the most sensitive position of the recorder a 1% deformation corresponds to a pen displacement of 25 cm. When the deformation of the specimen exceeded the maximum range of the extensometer, a constant speed chart drive was switched over to. The specimens were cyclically loaded to continuous higher loads and unloaded, until the 0.2% offset yield stress was exceeded. The cross-head speed used during the cyclic loading in the elastic and microplastic domain was 0.01 cm min^{-1}. Thereafter the specimens were loaded continuously to failure at a cross-head speed of $0.05\,cm\,min^{-1}$. The modulus of Young was determined on the recorded graphs as the initial slope in the elastic deformation zone. Subsequently the fracture surface of three different 50 μm fibre specimens was examined with a Cambridge scanning electron microscope. The density of the specimens studied was 41.8, 56.8, and 78.0%.

TABLE I The compaction pressure as a function of the density after sintering.

Compaction pressure ($MN\,m^{-2}$)	Density (%) after sintering at 1250° C	
	50 μm fibre specimen sintered for 2 h	100 μm fibre specimen sintered for 4 h
100	41.8	42.7
150	48.4	
200	56.8	56.0
400	72.1	70.9
600	78.2	78.9
800		84.5

Cylindrical compression specimens were compacted uniaxially with 50 and 100 μm diameter fibres. Specimens with densities varying between 35 and 80% were obtained. The diameter was 5.5 mm and the height varied between 6 and 6.5 mm. The sintering procedures for the 50 and 100 μm fibre specimens were identical to the ones used for the tensile specimens. The density was de-

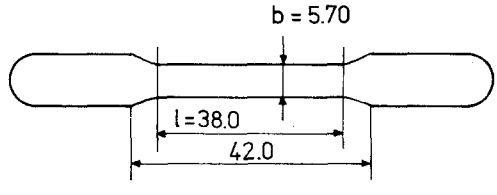

Figure 1 The tensile specimen used. Dimensions in mm.

TABLE II Results of the tensile tests on 50 μm fibre specimens

Specimen number	Thickness (mm)	Density (%)	0.01% offset yield stress ($MN\,m^{-2}$)	Young's modulus ($GN\,m^{-2}$)	UTS ($MN\,m^{-2}$)	Strain at fracture (%)
6	3.24	41.8	–	27.06	69	8.4
12	2.80	47.2	20.7	44.84	69	3.5
13	2.95	45.1	23.8	30.70	71	5.5
14	2.58	44.8	13.6	23.48	115	5.0
11	2.94	48.4	22.9	38.75	107	15
7	2.34	56.8	24.0	49.25	131	10.8
8	3.73	72.1	56.4	93.90	176	9.0
9	3.44	78.2	67.5	106.50	243	14.0
15	3.47	77.5	71.9	99.33	211	8.7
16	3.19	75.7	60.6	97.95	261	20
17	3.45	75.0	96.4	119.86	315	13

TABLE III Results of the tensile tests on 100 μm fibre specimens

Specimen number	Thickness (mm)	Density (%)	0.01% offset yield stress ($MN\,m^{-2}$)	Young's modulus ($GN\,m^{-2}$)	UTS ($MN\,m^{-2}$)	Strain at fracture (%)
2	5.58	42.7	10.4	20.32	52	9.0
1	4.37	56.0	34.7	61.87	123	9.3
18	4.37	56.7	23.3	42.32	120	18.5
19	4.10	57.1	23.5	54.06	130	20
20	4.29	57.2	24.5	40.96	111	11.5
3	3.52	70.9	48.4	90.78	196	14.3
21	3.39	71.1	46.6	98.74	226	23
22	3.60	69.6	39.0	97.66	203	24
23	3.60	69.4	42.5	119.92	198	12.8
4	3.13	78.9	58.3	119.50	300	27.3
5	2.96	84.5	92.6	158.33	359	23.7

termined geometrically. Compression testing was performed on the Instron TT-DM-L at a constant cross-head speed of $0.02\,cm\,min^{-1}$. The recorder chart was driven at a $2\,cm\,min^{-1}$ speed. Similar to the tension testing, the compression specimens were cyclically loaded to successively higher loads and unloaded. While unloading, the chart was driven in the opposite direction automatically.

3. Results and discussion

3.1. The modulus of elasticity measured in tension

The results of the tensile tests are summarized in Table II for the 50 μm fibre specimens and in Table III for the 100 μm fibre specimens. Linear regression analysis yields the correlations which are represented in Table IV.

Fig. 2 shows the established correlation between the density and the modulus of elasticity. High correlation coefficients were obtained (r = 0.98 and 0.96 for the 50 and 100 μm fibre specimens respectively.)

TABLE IV Results of the linear regression analysis with data from the tensile tests. Young's modulus, the yield stress and the density are expressed in $GN\,m^{-2}$, $MN\,m^{-2}$ and % respectively.

	Y	A_1	A_2	X	R	K
50 μm fibre specimens	E	− 74.29	2.34	dens.	0.98	11
	$\sigma_{0.01}$	− 62.4	1.7	dens.	0.91	10
100 μm fibre specimens	E	−132.98	3.32	dens.	0.96	11
	$\sigma_{0.01}$	− 69.9	1.7	dens.	0.92	11
100 μm fibre specimens including 100% density	E	−134.64	3.34	dens.	0.98	12

A_1 and A_2 are the constants of the linear relation

$$Y = A_1 + A_2 X$$

R is the correlation coefficient, a value close to 1 indicating a high degree of correlation. K is the number of representation points used for the particular correlation.

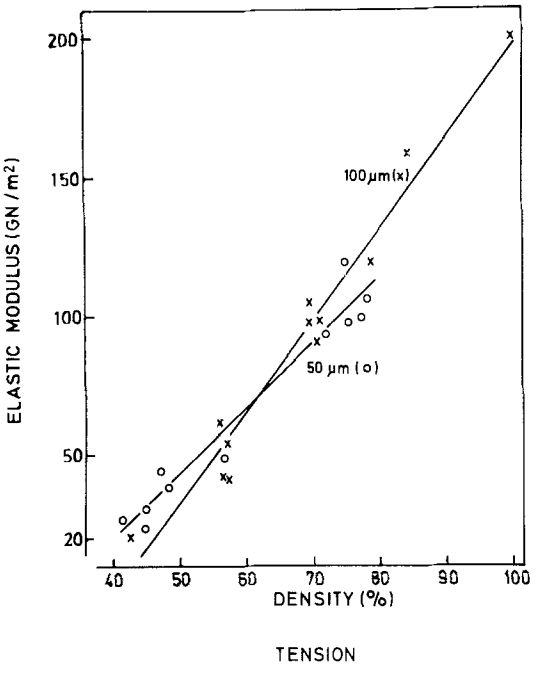

Figure 2 The variation of the modulus of elasticity, measured in tension, as a function of the density for 50 and 100 μm fibre specimens.

The experimental results can be compared with the theoretical relations for the variation of the elastic constants of porous materials and of composites. Mackenzie [20] established an equation for the relation between the elastic constants and the density of porous materials, assuming spherical closed pores. For closed pores in a continuous matrix with a typical Poisson's ratio of $\nu = 0.3$ the change in elasticity can be adequately represented [21] by the equation:

$$E_M = E_0(1 - 1.9P + 0.9P^2)$$

with E_M = the modulus of elasticity according to the Mackenzie theory,
E_0 = the modulus of elasticity of the 100% dense material,
P = the fractional porosity.

Several theories exist which relate the variation of the composition of a composite with its elastic moduli. Two rather rough models consider the composite being composed of elements experiencing a uniform strain (the Voigt model) or a uniform stress (the Reuss model). Hill [22] has shown that these two models respectively provide a rigorous upper and lower bound for the actual variation of the elastic moduli. Considering the porous materials as composites made of fibre and pores, the Voigt and Reuss models are reduced to the equations:

$$E_V = E_0 \cdot d$$

$$E_R = 0$$

with E_V, E_R = the modulus of elasticity according to the Voigt and Reuss theory,
d = the fractional density.

A third and more precise model was elaborated by Hashin and Shtrikman [23]. They assumed a macroscopically homogeneous, and isotropic system composed by a matrix with elastic, homogeneous and isotropic inclusions. An arbitrary shape was accorded to the included phases. Using variational principles much closer bounds were obtained. Applying the bounds to porous materials, one obtains:

$$E_L = 0$$

$$E_U = \frac{9K_U G_U}{3K_U + G_U}$$

$$K_U = K + \frac{1-d}{-(1/K) + [3d/(3K+4G)]}$$

$$G_U = G + \frac{1-d}{-(1/G) + [6(K+2G)d/5(3K+4G)G]}$$

with the indices U and L indicating the upper and lower bounds, K the bulk modulus, and G the shear modulus.

The Mackenzie theory bears an immediate advantage with regard to the Hashin–Shtrikman theory: the presence of the pores is taken into account in the model. However, it was assumed that the pores were spherical and did not interconnect. This is unlike the presently discussed porous structures.

The Mackenzie relation, the Voigt, Reuss and Hashin–Shtrikman bounds of porous stainless steel AISI 316 L and the experimentally obtained correlations between the Young's modulus and the density are plotted in Fig. 3. The theoretical relationships were calculated, using the values $E = 195.2\,\mathrm{GN\,m^{-2}}$ and $G = 78.0\,\mathrm{GN\,m^{-2}}$ [25].

The results of Bal'shin and Fedotov [24], who measured with an "Elastomat" the Young's modulus of porous specimens made of "Kh 18 N9I" stainless steel fibres with diameter of 50 μm and length 7 mm, are also represented in Fig. 3.

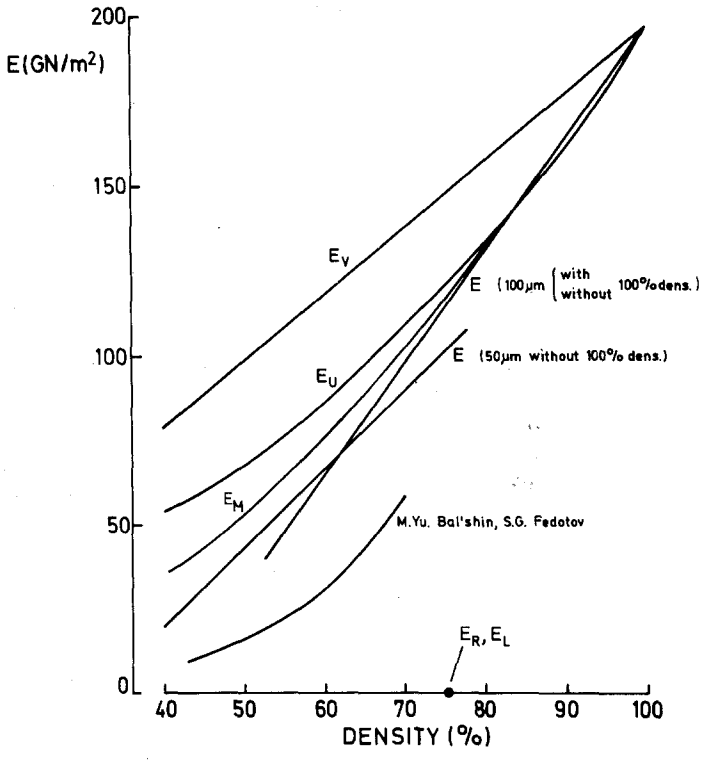

Figure 3 Comparison of the variation of the modulus of elasticity as a function of the density, among theoretical models, own results and literature data.

From Fig. 3, it is evident that the experimentally determined lines are best approached by the theoretical Mackenzie curve. It should be noted, however, that there are departures between the straight lines determined by the regression analysis of the experimental data points and the theoretical Mackenzie curve. For the 50 μm fibre compacts an increasing difference is noted with increasing density; for the 100 μm fibre specimens the difference is most pronounced at lower densities. It is apparent that the ranges of good agreement between the experimental straight lines and the Mackenzie curve correspond to the range of the experimental densities. Half the number of 50 μm fibre compacts has a density equal to or less than 55%. All but one of the 100 μm fibre specimens have a density equal to or larger than 55%. As such, the established linear relationships between the density and the modulus of elasticity are valid within their experimental density range only.

For smaller densities the differences between the experimental values and those predicted by the Mackenzie theory can be explained as follows. At larger densities the elastic deformation of the fibres is spatially hindered by the sinter bonds. As such the metal fibres deform in a manner similar to a 100% dense metal. With increasing porosity the spatial hindrance is reduced, thus allowing the fibres to be elastically elongated as well as elastically aligned in the tensile direction. This deformation was not accounted for in the Mackenzie model. The upper Hashin–Shtrikman bound is also a close bound to the variation of Young's modulus with the density. The condition of uniform strain which leads to the determination of the upper bound is thus a predominant deformation feature of the present porous structures, at least at higher densities.

The results of Bal'shin and Fedotov which are also shown in Fig. 3 are appreciably different from ours. The difference is, however, very hard to explain because these authors did not report in sufficient detail on the material used and the experimental procedure.

3.2. The yield stress in tensile testing

The yield stress measured in tension with the 50 μm and the 100 μm fibre compacts has been given in Tables II and III. A correlation between the yield stress and the density has been shown by linear regression analysis; the results of these analyses are given in Table IV. As shown in Fig. 4, the correlation between the yield stress and the

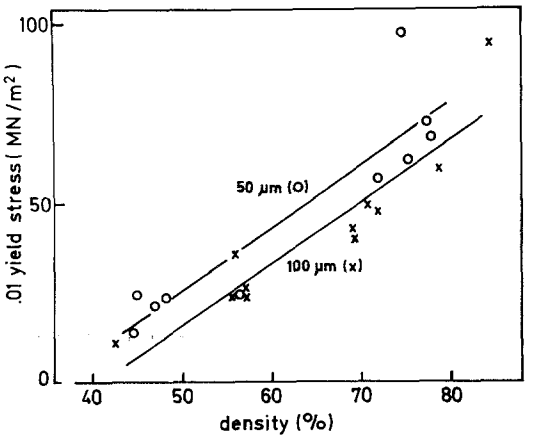

Figure 4 The variation of the yield strength as a function of the density for 50 and 100 μm fibre specimens.

density for 50 and 100 μm fibre tensile specimens gives parallel straight lines, the one for the 100 μm fibre specimens being lower.

The yield stress is determined by the onset of plastic deformation of the fibres. Assuming that upon uniaxial tension the fibres are elongated or bent, yielding of the porous structures occurs at the onset of plastic elongation of the fibres or at the start of plastic bending of the fibres, or both.

The difference between the yield stress of the 50 and 100 μm fibre specimens is most probably due to the onset of plastic bending of some fibres. For the same spatial arrangement of the fibres, an external load produces a bending moment which leads to plastic deformation of the 100 μm fibres at half the value needed for deformation of the 50 μm fibres.

3.3. Tensile fracture mode

An important question regarding the porous metal fibre structures is whether the eventual failure is a rupture of sintered bonds or a fracture through the fibres. Although the temperature and time of sintering are quite high, they do not yield an optimized sintered aggregate: e.g., a sintering at 1300° C for 4 h would be required for the 50 μm fibre specimens [26].

A study of the fracture surfaces of the 50 μm fibre specimens with the SEM shows that they fail by a ductile fracture of the fibres except at the lower densities where tearing of sintered bonds occurs. Scanning electron micrographs of the fracture surfaces of the specimens with different density are given in Figs. 5a and b. At 41.8% density ruptured sintered bonds and fractured fibres are apparent (Fig. 6), but is apparent from Fig. 5a that the fracture proceeds primarily through the fibres and not through the sintered bonds. At 56.8% and 78.0% density the aspect of teared sintered bonds is unseen (Fig. 5b); failure occurs by ductile fracture of the fibres (Fig. 7).

3.4. The modulus of elasticity measured in compression

A typical compression recording is shown in Fig. 8. Three stages can be discerned systematically. All three stages correspond to a plastic

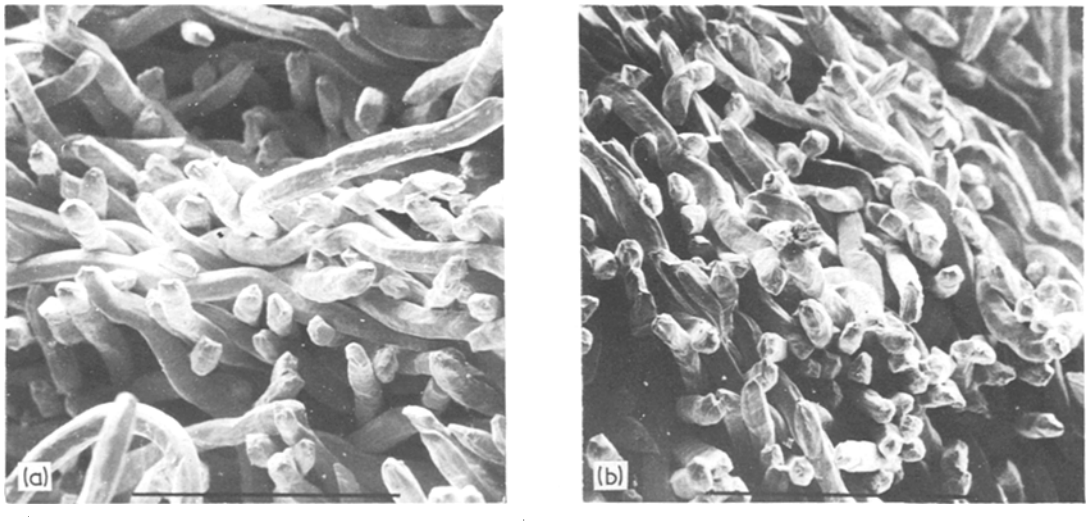

Figure 5 (a) and (b) Scanning electron micrograph of the fracture surfaces of 50 μm fibre specimens with densities of 41.8 and 56.8% respectively (84 ×).

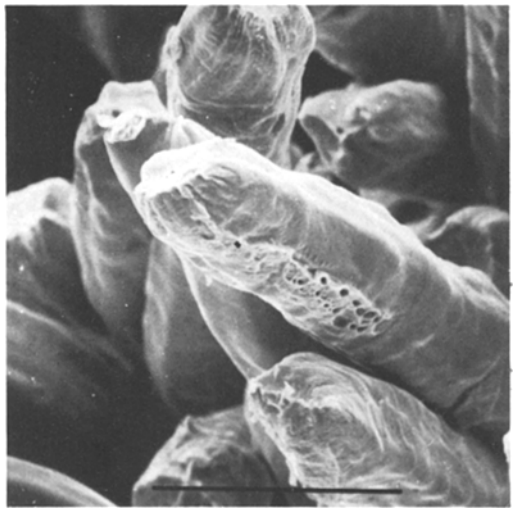

Figure 6 Detail of the fracture surface of a tensile specimen of 41.8% density: the central fibre is ruptured and its sinter bond is torn (× 440).

deformation of the specimen. This is apparent from the compression graphs, where upon unloading a permanent deformation is observed. The deformation calculated from the graph is the same as the deformation measured on the tested specimen. The different slope between loading and unloading is not due to an elastic after effect. One week after the original compression test three specimens were tested again under identical conditions. This showed that compressing the specimen to stresses lower than the maximum stress of the first testing yields a reversible deformation.

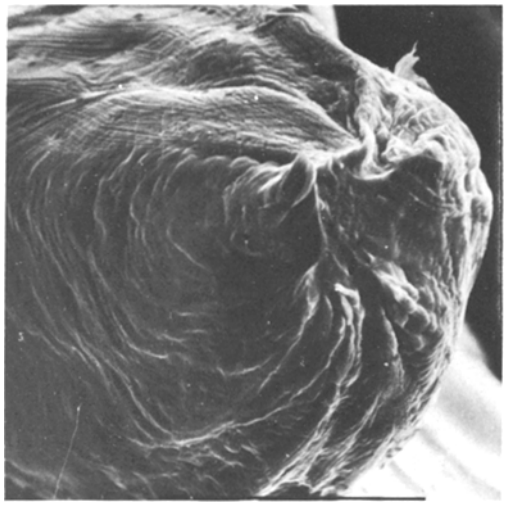

Figure 7 Detail of the ductile failure of fibres (× 1700).

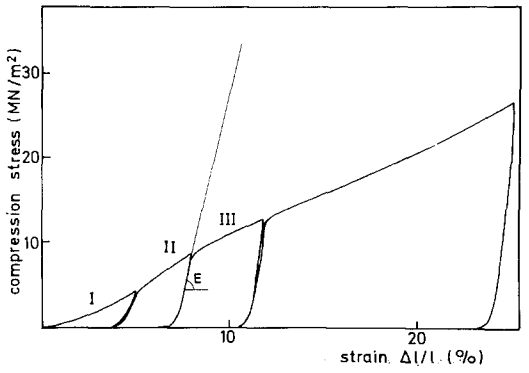

Figure 8 A typical graph recorded upon compression.

The deformation during the different stages probably follows this pattern: in stage I the bottom and top surfaces of the specimen are compressed to perfectly parallel surfaces. In stage II some fibres are plastically deformed, but others only elastically. Subsequently all fibres are plastically deformed in stage III.

The pressure required for plastic deformation of the sintered specimen at a given density is substantially smaller than the pressure to compact the unsintered fibres to the identical green density.

The sintering step thus eliminates the work hardening caused by the compaction. Upon compression testing the plastic deformation leads to an increase in density of the specimen. The increase is small at the end of stage II (1% at the mean). In stage III, however, a substantial increase is noted: the pressure increment to yield a given increase in density is four times larger in stage II than in stage III deformation.

The modulus of elasticity of the compression specimens was determined as the slope of the unloading graph at the end of stage II deformation (cf. Fig. 8). The measured values were plotted versus the initial density in Fig. 9. The linear relationships established by a least-squares regression analysis were:

50 μm fibre specimens (20 data points)

$$E = -6.53 + 0.208\,d \quad r = 0.99$$

100 μm fibre specimens (23 data points)

$$E = -6.70 + 0.196\,d \quad r = 0.98$$

with E = the modulus of elasticity in GN m^{-2},
d = the density in %
r = the correlation coefficient.

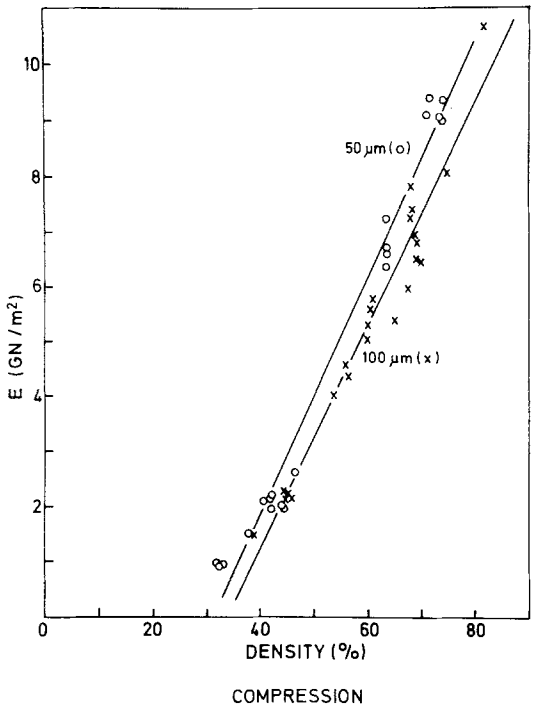

Figure 9 The variation of the modulus of elasticity, measured in compression, as a function of density.

Comparing the modulus of elasticity as obtained by compression with the one measured by tension testing, it is apparent that the former is about ten times smaller than the latter. This discrepancy is explained by the deformation behaviour of the fibres, which is depicted schematically in Fig. 10. Upon tensile testing many fibres are elastically stretched, unlike in compression testing where the fibres are bent. Macroscopically this results in a much reduced modulus of elasticity upon compression.

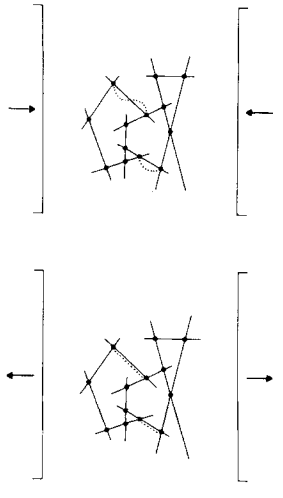

Figure 10 Schematic representation of the main deformation pattern of the fibres upon tension and compression testing.

Rostoker *et al.* [27] measured moduli of elasticity of pre-kinked titanium and wrought cobalt–chromium alloy fibres by tension and compression tests. They obtained values for tension and compression which did not differ markedly. Their values were within the same range as our experimental results in compression. Comparing with our results, the lower value of Young's modulus in tension is to be attributed to the straightening of the pre-kinked fibres which were used by these authors.

4. Conclusions

The variation of the modulus of elasticity measured in tension is best approached by the theoretical Mackenzie relationship. The upper Hashin–Shtrikman bound also represents a close bound. Upon compression the modulus of elasticity is lowered by a factor of ten. The value upon compression is close to Young's modulus of the spongy bone which surrounds the prosthetic porous coatings. Failure in service of the porous coating by tearing of sintered bonds is unlikely when the density of 50 μm fibre coatings exceeds 56%.

Acknowledgements

The metal fibres used in this study were kindly provided by N. V. Bekaert, Zwevegem, Belgium.

References

1. H. GOEMINNE, R. DE BRUYNE, J. ROOS and E. AERNOUDT, *J. Filtration and Separation* (1974) 351.
2. V. A. TRACEY, Transactions of the 4th European Conference on Powder Metallurgy, Grenoble, France (1975) p.p. 144–165.
3. J. GALANTE, W. ROSTOKER, R. LUECK and R. D. RAY, *J. Bone Joint Surg.* **53A** (1971) 101.
4. P. DUCHEYNE, M. MARTENS, P. DE MEESTER, E. AERNOUDT and J. C. MULIER, *J. Biomed. Mater. Res.* **11** (1977) 811.
5. S. F. HULBERT, F. A. YOUNG, R. S. MATHEWS, J. J. KLAWITTER, C. D. TALBERT and F. H. STELLING, *ibid.* **4** (1970) 433.
6. H. HAHN and W. PALICH, *ibid.* **4** (1970) 571.
7. R. M. PILLIAR, H. U. CAMERON and I. MACNAB, *Biomed. Eng.* **10** (1975) 126.
8. M. R. DUSTOOR and J. S. HIRSCHHORN, *Powder Met. Int.* **5** (1973) 183.

9. K. R. WHEELER, R. P. MARSHALL and K. R. SUMP, *Biomater., Med. Dev, Art. Organs* **1** (1973) 337.
10. J. GALANTE and W. ROSTOKER, *J. Biomed. Mater. Res. Symp.* 7 (1973) 43.
11. P. DUCHEYNE, E. AERNOUDT, M. MARTENS, J. C. MULIER and P. DE MEESTER, Proceedings of the 4th European Conf. on Powder Metallurgy, Grenoble (Société française de Métallurgie, Paris, 1975).
12. R. P. WELSH, R. M. PILLIAR and I. MACNAB, *J. Bone Joint Surg.* **53A** (1971) 963.
13. P. DUCHEYNE, Ph. D. thesis, Katholieke Universiteit Leuven (1976).
14. J. P. PAUL and J. POULSON, Proceedings of the 5th International Conference of Experimental Stress Analysis, Udine, Italy (1974).
15. P. DUCHEYNE, P. DE MEESTER, E. AERNOUDT, M. MARTENS and J. C. MULIER, *J. Biomed. Mater. Res. Symp.* 9 (1975) 199.
16. K. L. MARKOLF and H. C. AMSTUTZ, *J. Biomechanics* 9 (1976) 73.
17. J. C. BEHRENS, P. S. WALKER and H. SHOJI, *J. Biomechanics* 7 (1974) 201.
18. P. DUCHEYNE, L. HEYMANS, M. MARTENS, E. AERNOUDT, P. DE MEESTER and J. C. MULIER, *J. Biomechanics* **10** (1977) 747.
19. P. DUCHEYNE, E. AERNOUDT, P. DE MEESTER, M. MARTENS, J. C. MULIER and D. VAN LEEUWEN, *ibid.* (submitted).
20. J. K. MACKENZIE, *Proc. Phys. Soc. (London)* **B63** (1950) 2.
21. W. D. KINGERY, "Introduction to Ceramics", (John Wiley & Sons, New York, 1960) p. 598.
22. R. HILL, *J. Mech. Phys. Solids* **11** (1963) 357.
23. Z. HASHIN and S. SHTRIKMAN, *ibid* **11** (1963) 127.
24. M. Yu. BAL'SHIN and S. G. FEDOTOV, *Sov. Powder Met.* **64** (1968) 310.
25. F. GAROFALO, P. R. MALENOCK and G. V. SMITH, ASTM Symposium on the determination of elastic constants, June 1952.
26. H. GOEMINNE, R. DE BRUYNE and J. ROOS, Proceedings of the 4th European Conference on Powder Metallurgy, Grenoble (Société française de Métallurgie, Paris, 1975).
27. W. ROSTOKER, J. O. GALANTE and G. SHEN, *J. Test. Eval.* **2** (1974) 107.

Received 14 March and accepted 3 May 1978.